Available online at www.sciencedirect.com

SciVerse ScienceDirect

Acta Materialia 60 (2012) 1999–2006

Acta MATERIALIA

www.elsevier.com/locate/actamat

Leaf-like dislocation substructures and the decrease of martensitic start temperatures: A new explanation for functional fatigue during thermally induced martensitic transformations in coarse-grained Ni-rich Ti–Ni shape memory alloys

Jian Zhang [a,b,c,*], Christoph Somsen [a], Tobias Simon [a], Xiangdong Ding [b], Sen Hou [b], Shuai Ren [b], Xiaobing Ren [b,c], Gunther Eggeler [a,b], Kazuhiro Otsuka [b,c], Jun Sun [b]

[a] *Institute for Materials, Ruhr-Universität Bochum, 44780 Bochum, Germany*

[b] *Multi-disciplinary Materials Research Center, Frontier Institute of Science and Technology, State Key Laboratory for Mechanical Behaviour of Materials, Xi'an Jiaotong University, 710049 Xi'an, China*

[c] *National Institute for Materials Science, 1-2-1 Sengen, 305-0047 Tsukuba, Ibaraki, Japan*

Received 26 October 2011; received in revised form 7 December 2011; accepted 8 December 2011
Available online 1 March 2012

Abstract

During repeatedly imposed thermally induced martensitic transformations in Ti–Ni shape memory alloys, the martensite start temperature M_s decreases. This has been rationalized on the basis of a scenario where an increasing dislocation density makes it more and more difficult for martensite to form. However, it is not clear why dislocations which form because they accommodate the growth of martensite during the first cooling cycle should act as obstacles during subsequent transformation cycles. In the present work we use diffraction contrast transmission electron microscopy to monitor the formation of unique leaf-like dislocation substructures which form as the martensite start temperature decreases during thermal cycling. We interpret our microstructural results on the basis of a microstructural scenario where dislocations play different roles with respect to the propagation of a big martensite needle in one transformation cycle and the nucleation and growth of new martensite needles in the following cycles. As a consequence, chestnut-leaf-like dislocation arrays spread out in different crystallographic directions.

Keywords: Ti–Ni shape memory alloys; Martensitic transformations; Leaf-like dislocations substructures; Dislocations; Functional fatigue

1. Introduction

Ti–Ni alloys are the commercially most successful shape memory alloys (SMAs). They show the one-way effect (1WE) and pseudo-elasticity (PE), both of which are exploited in various applications [1–4]. Both effects rely on martensitic transformation, which is a diffusionless phase transformation that can be induced thermally and mechanically [4–6]. Atomic, thermodynamic, crystallographic and micromechanical aspects of the martensitic transformation have been extensively discussed in the literature [7–11] and the associated research fields (martensitic transformations and shape memory alloys) have reached a high level [4,12].

Shape memory components typically operate under cyclic conditions. They are typically subjected to alternating temperatures, cyclic stresses or both [7–9,12]. Today it is known that cyclic operation conditions result in functional fatigue [5]. The martensite start temperature (M_s) in a 1WE application and the critical stress (σ_c) in a PE application are not constants. They evolve during thermal and mechanical

* Corresponding author at: Institute for Materials, Ruhr-Universität Bochum, 44780 Bochum, Germany. Tel.: +49 234 32 29159; fax: +49 234 32 14235.
E-mail address: zhang.jian@rub.de (J. Zhang).

1359-6454/$36.00 © 2011 Acta Materialia Inc. Published by Elsevier Ltd. All rights reserved.
doi:10.1016/j.actamat.2011.12.014

cycling. Materials scientists intuitively associated this with increasing dislocation densities.

It is well known that dislocations are lattice defects which can help to accommodate elastic stresses associated with the formation of martensite [13,14]. But they can also act as obstacles. Thus it is well known that strong cold work suppresses martensitic transformation [15]. During thermal cycling of SMAs, M_s was reported to decrease and this suggests that dislocation plasticity makes it difficult for martensite to form ("bad plasticity") [8,9]. On the other hand, it is well known, that the critical stress required to form stress-induced martensite decreases. Here dislocation reactions appear to promote the martensitic transformation ("good plasticity") [16,17]. These well-known facts show that the physical nature of functional fatigue in 1WE and PE applications cannot simply be rationalized invoking an average dislocation density argument.

Here we focus on the decrease of M_s during thermal cycling, as described by several authors (e.g. Refs. [8,9]). Recently, the elementary processes which govern the creation of dislocations during the martensitic transformation received close attention [12,18–21]. For Ti–Ni it was shown that the dislocations had Burgers vectors of type $b = a\langle 001\rangle$ [18]. Simon et al. [12] suggested a microstructural scenario which explained the increase of dislocation line length by emission of additional dislocation loops from an ingrown dislocation segment triggered by the stress field of an approaching martensite needle.

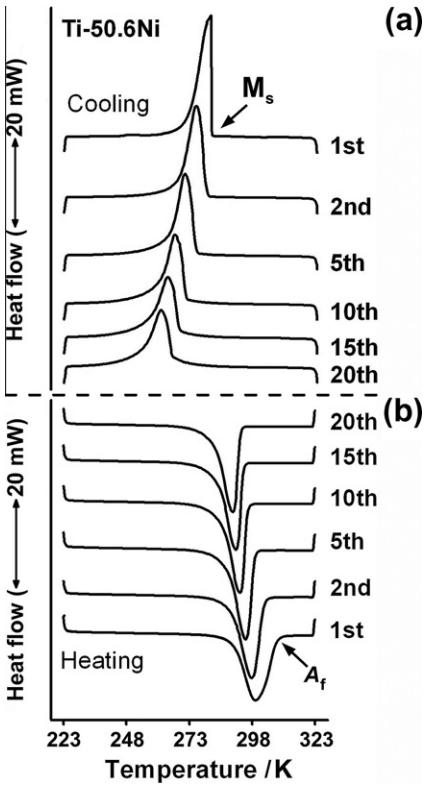

Fig. 1. DSC charts of Ti–50.6Ni recorded during (a) cooling, and (b) heating.

At present it is not clear why dislocations, which form to accommodate the growth of martensite during the first cooling cycle, act as obstacles during the next transformation cycle. Why the formation of thermally and stress-induced martensites react differently to increasing dislocation densities is not clear. It strongly suggests that the parameters which characterize the associated dislocation substructures are important. In the present study, we make an effort to explain the decrease of M_s during thermal cycling in terms of an evolving dislocation substructure.

2. Material and experiments

A 0.5 mm coarse-grained Ti–50.6Ni sheet (nominal composition in at.%) with an M_s below room temperature was studied. Small cylinders with diameters of 5 mm and masses of 40 mg were spark-eroded, and sealed in evacuated quartz tubes. The cylinders were then solution-annealed at 1273 K for 1 h followed by subsequent water-quenching as described earlier [22]. After solution annealing, the samples were chemically etched to remove thin oxide layers.

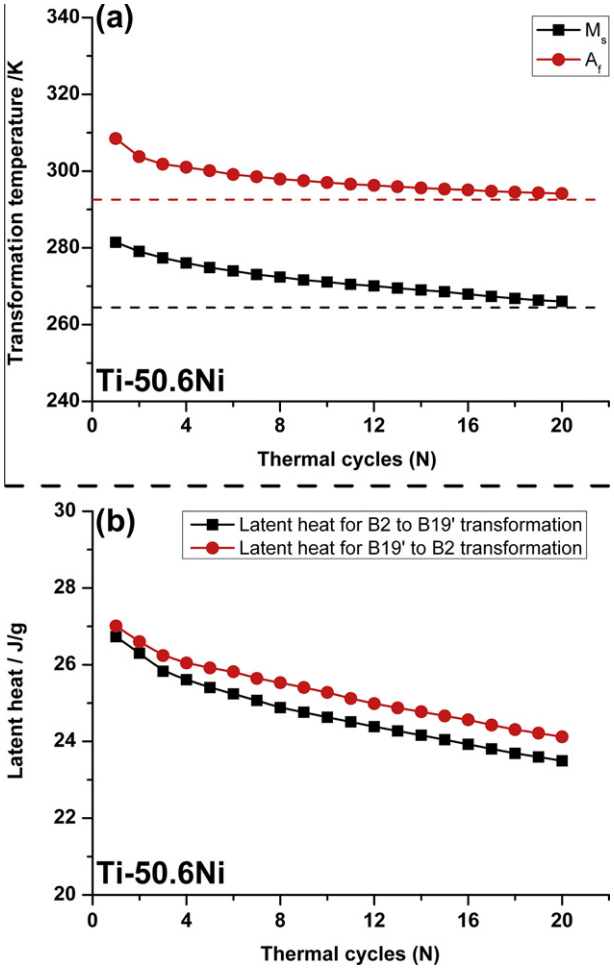

Fig. 2. Effect of thermal cycling on functional properties. (a) Evolution of M_s and A_f. (b) Decrease of latent heats associated with the formation of martensite (on cooling) and austenite (on heating).

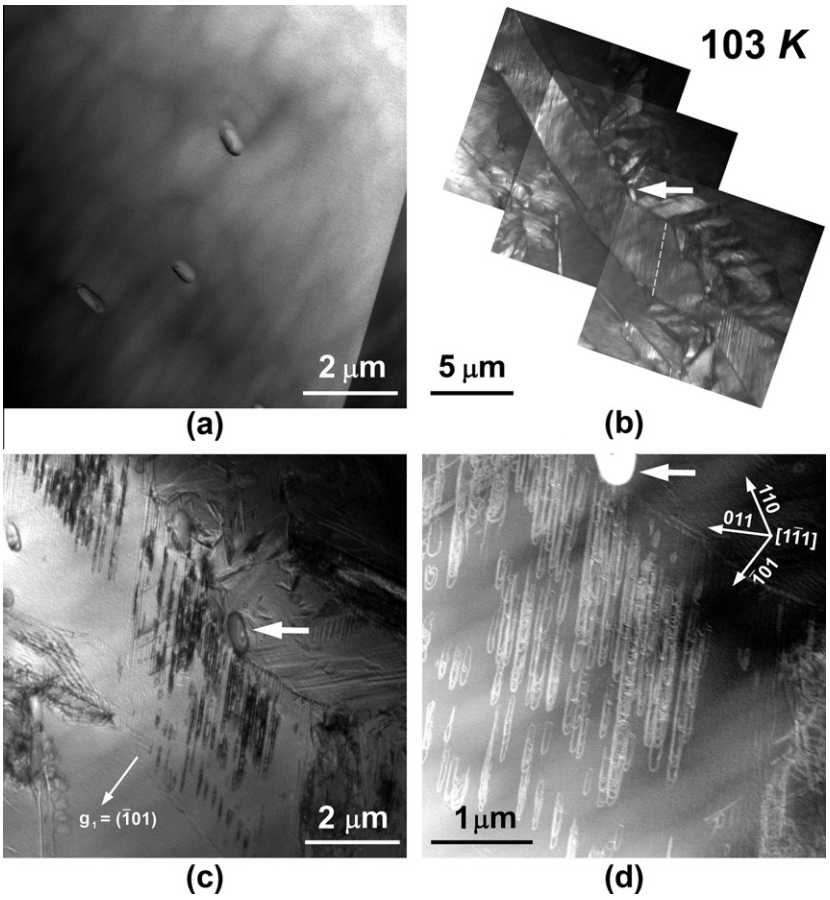

Fig. 3. TEM experiments which prove the formation of dislocations during a martensitic transformation. (a) Dislocation-free austenite at room temperature. (b) Martensite needle with fine twins, which has formed during cooling to 103 K. (c) Dislocations after reheating to 353 K observed at room temperature (diffraction contrast). (d) Dislocations after reheating observed at room temperature (STEM mode).

Thermal cycling was then carried out in a differential scanning calorimeter (DSC) of type Q200, TA. The DSC tests were performed at a cooling/heating rate of 10 K min^{-1}. For one thermal cycle the samples were first heated up to a temperature of 323 K, held for 2 min followed by subsequent cooling to 223 K. Then the samples were held for 2 min and heated up to 323 K. Specimens were subjected to 1, 5, 10 and 20 DSC cycles. Their microstructures and the microstructure of the as-solutionized sheet material were subsequently investigated using transmission electron microscopy (TEM).

An FEI Tecnai F20G^2 with a HAADF (high angle annular dark field) detector was used to study the microstructures of the virgin cylinder and of the specimens subjected to DSC cycling. One in situ cooling/heating experiment was performed using a Phillips CM20 TEM, equipped with a Gatan 636HD cooling/heating holder. Both microscopes were operated at 200 kV. Thin TEM foils were prepared from 5 mm disks which were mechanically polished down to a thickness of ~120 μm. These disks were subsequently electro-polished using a standard double-jet procedure (TenuPol-5, Struers) with an electrolyte consisting of 20% sulfuric acid and 80% methanol. Electro-polishing was performed at 288 K at a voltage of 30 V.

3. Results

3.1. Evolution of DSC chart features

In the DSC experiments performed in the present study, our Ti–50.6Ni alloy shows one step transformations on cooling and heating, Fig. 1. One exothermic DSC peak on cooling is associated with the forward transformation from B2 to B19′, Fig. 1a. An endothermic peak on heating is related to the heat flow corresponding to the reverse transformation, Fig. 1b. During thermal cycling, both peaks shift towards lower temperatures. Fig. 2a shows the evolution of the martensite start temperature M_s and the austenite finish temperature A_f during thermal cycling. These two characteristic temperatures are commonly referred to when discussing martensitic forward and reverse transformations in Ti–Ni. M_s and A_f decrease during thermal cycling, Fig. 2a. Fig. 2a suggests that both temperatures significantly decrease during the early cycles and eventually reach a constant value. Fig. 2b shows a plot of the latent heats evaluated from the areas under the DSC peaks in Fig. 1. Fig. 2b shows that the intensity of both heat effects associated with the forward and reverse transformations slightly decreases during cycling (effect < 10%).

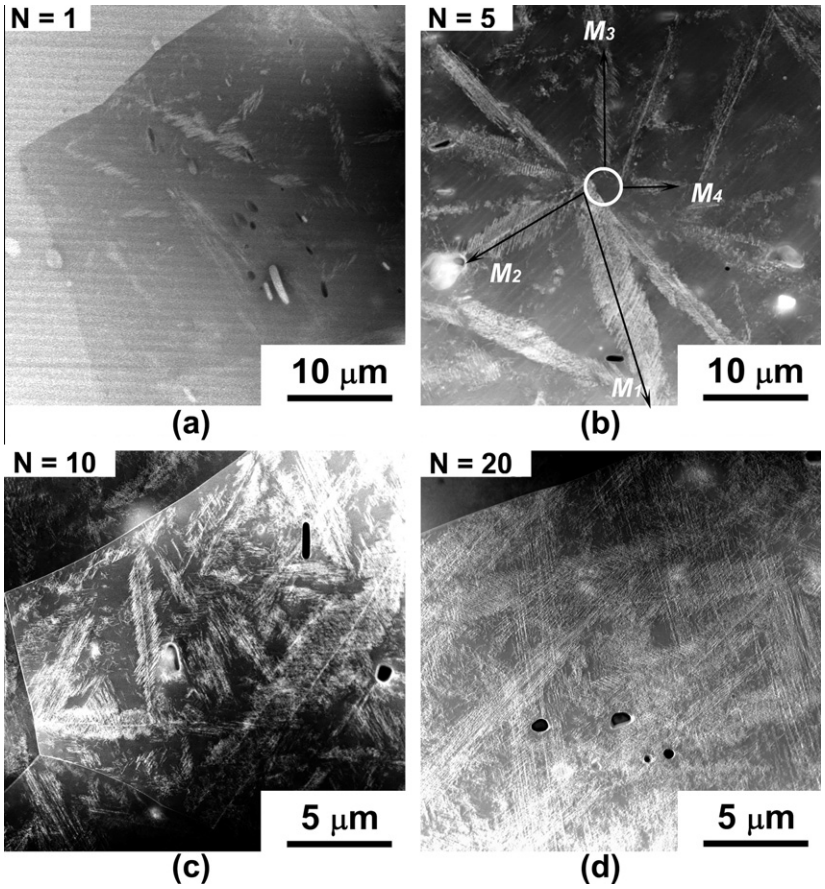

Fig. 4. Overview TEM micrographs (STEM and HAADF) taken from Ti–50.6Ni specimens which were subjected to different numbers N of thermal cycles. (a) $N = 1$. (b) $N = 5$. (c) $N = 10$. (d) $N = 20$. In (b), four black arrows marked with $M1$, $M2$, $M3$ and $M4$ denote four martensite needles, which generated the four corresponding dislocation leaves in the image as the real analogy to martensite needles and dislocation leaves schematically shown in Fig. 7.

3.2. Formation of dislocation loops

One in situ cooling/heating experiment was performed on a virgin sample in order to prove that dislocation substructures form during the martensitic transformation and that the spatial features of the dislocation substructure are related to the needle-like martensite geometry. The TEM micrographs shown in Fig. 3a and b were taken during an in situ TEM cooling experiment in the Philips CM20. Fig. 3c and d shows the post mortem micrographs of the microstructure after heating back to the austenite regime in the FEI Tecnai F20G^2.

Fig. 3a shows a TEM micrograph of the austenitic material state prior to cooling. It can be clearly seen that the austenitic microstructure is free of dislocations. Fig. 3b shows a montage of micrographs of another region of the same grain after cooling down to 103 K. The microstructure is now martensitic, which was proven by electron diffraction (not shown here). One inclusion in the center of the image is marked with a white arrow for reference. A large martensite needle extends from the upper left to the lower right of the image. Fine lines in the martensite needle indicate the presence of twins and/or twin-related martensite variants. The direction of the corresponding interfaces is indicated by one fine dashed line. The martensitic material in Fig. 3b was subsequently heated back to 353 K in order to re-establish the austenite state.

Fig. 3c and d shows the dislocation substructure, which has formed as a result of the martensitic transformation (two-beam TEM contrast and STEM mode). Care was taken to ensure that the orientation of the specimen in Fig. 3a and b (in the CM20) was the same as in Fig. 3c. Fig. 3c was taken at a g-vector of $(\bar{1}\,0\,1)$. Elongated dislocation loops can be recognized with directions which match the directions of the fine twins highlighted in the large martensite needle in Fig. 3b. It should be noted that Fig. 3c was taken at a higher magnification than Fig. 3b. It appears that each elongated dislocation loop is related to one fine martensite twin. The dislocations were subsequently investigated in the STEM mode, which yields a very good contrast as shown in Fig. 3d. Tilt experiments showed that the Burgers vectors of the dislocations were of type $a[0\,0\,1]$, in agreement with what has been previously reported in the literature [12,18].

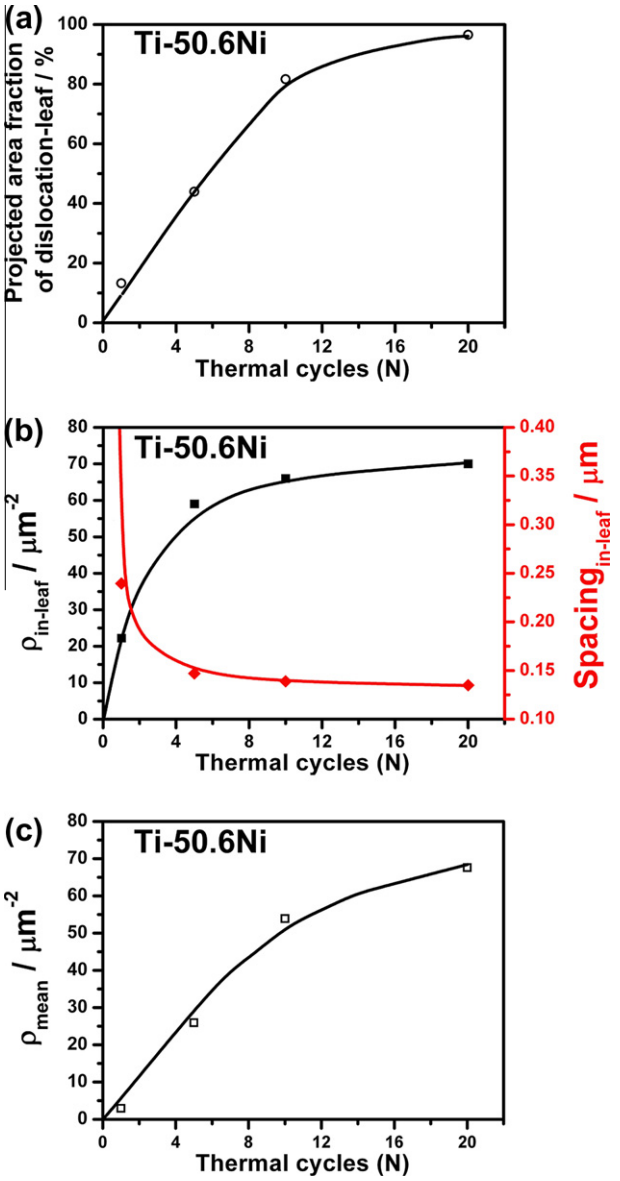

Fig. 5. Evolution of dislocation substructure during thermal cycle. (a) Increase of the projected area fraction of dislocation leaf (○). (b) Increase/decrease of the dislocation density (■) /dislocation spacing (♦) in leaves. (c) Increase of mean dislocation density (□) during thermal cycling.

3.3. Evolution of dislocation substructures

For the objectives of the present study it is important to document how dislocation substructures evolve during thermal cycling. For this purpose we investigate specimens which have been subjected to 1, 5, 10 and 20 DSC cycles in the TEM. TEM micrographs are presented in Fig. 4, where we use lower magnifications which allow assessing larger areas of the specimens. Fig. 4a shows the micrograph of the material after one thermal cycle. From what has been reported in Fig. 3 we know that the dislocations form clusters with leaf-like geometrical features which are governed by the geometry of martensite needles. Several such isolated dislocation leaves are spread over the specimen area after one thermal cycle. Fig. 4b shows the microstructure after five cycles. Chestnut-leaf-like dislocation arrays have spread out from a common center (highlighted with a white circle) in different crystallographic directions (highlighted with black arrows). After 10 cycles more leaves have formed, Fig. 4c. And after 20 cycles, the leaf density is so high (Fig. 4d), that it is difficult to distinguish individual leaves. Fig. 5 summarizes some quantitative metallographic results. In Fig. 5a we present the projected area fraction of dislocation leaves which increases during cycling. Fig. 5b shows that the dislocation density within the leaves $\rho_{in\text{-}leaf}$ increases during thermal cycling. This corresponds to a decrease of dislocation spacing in the leaves during thermal cycling, Fig. 5b. We combine the information presented in Fig. 5a and b to document the increase of the mean dislocation density ρ_{mean} during thermal cycling, Fig. 5c.

4. Discussions

4.1. Formation of dislocations

In the present study we investigate the formation of dislocations in one grain of a coarse-grained Ti–50.6Ni alloy. In Section 3.2 we have shown that the formation of dislocations accompanies the martensitic transformation. The fine scale features of elongated dislocation loops suggest that there is a close relation between these dislocations and the fine accommodation twins in the martensite needle, as schematically illustrated in Fig. 6. Fig. 6a shows how a martensite needle grows in an austenitic region. Upon further cooling as in Fig. 6b the needle has grown and dislocations have formed which keep the overall elastic strain energy at a minimum. Finally, in Fig. 6c the needle retreats on heating and leaves dislocations behind. This rationalizes our experimental observations reported in Fig. 3. So far our results are in line with what has been reported by

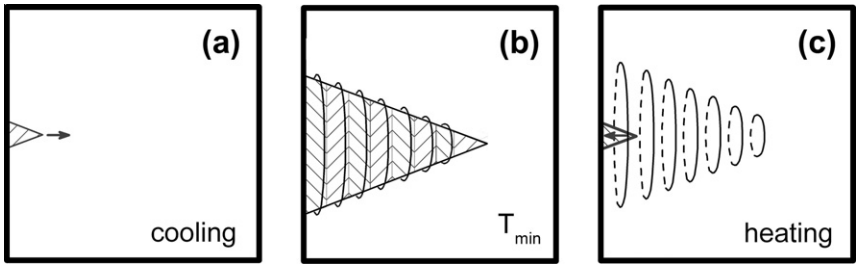

Fig. 6. Schematic illustration for explaining how a martensite needle creates a dislocation leaf.

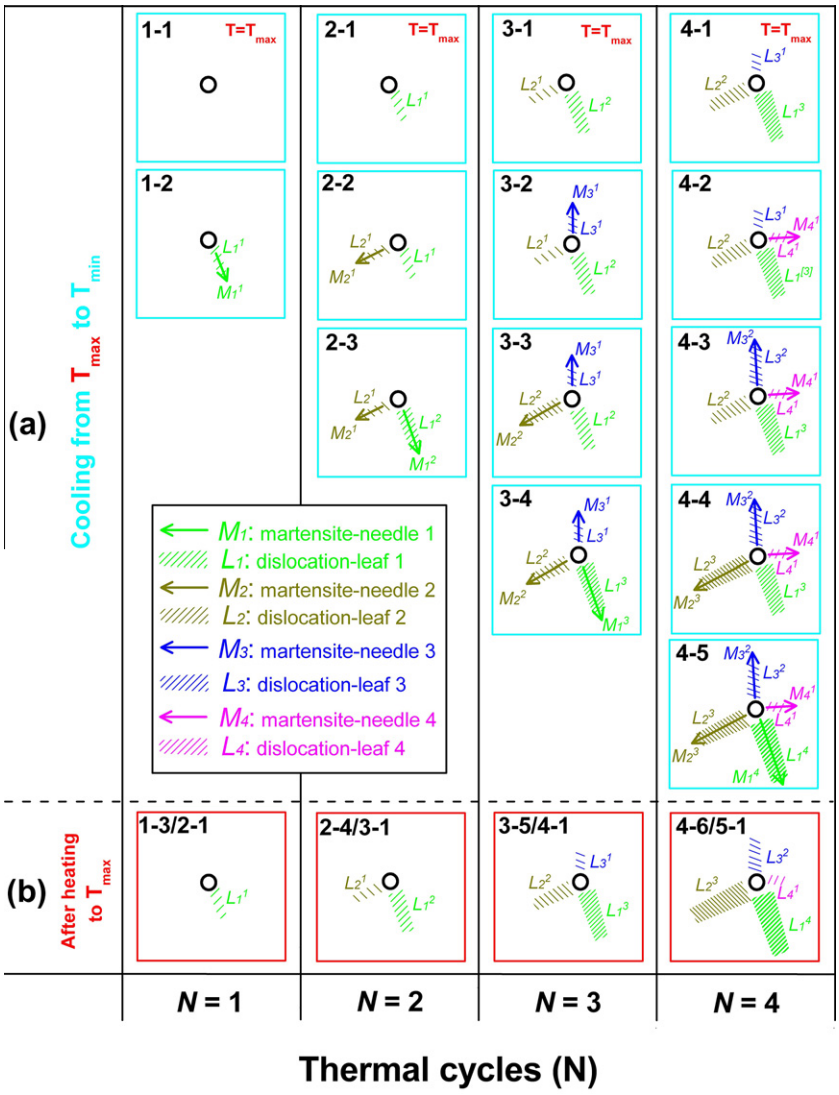

Fig. 7. Schematic explanation of M_s^{alloy} decrease during thermal cycling between the maximum temperature (T_{max}) and the minimum temperature (T_{min}) on the basis of the creation and evolution of dislocation leaves. (a) Illustrations of the microscopic evolution during cooling parts of the first four thermal cycles. (b) Illustrations of the microscopic evolution at T_{max} of the first four thermal cycles. The black circles in (a) and (b) denote one nucleation site. Four arrows and four raster-like patterns of different color stand for the martensite needles and the corresponding dislocation leaves, as depicted in the inset of (a).

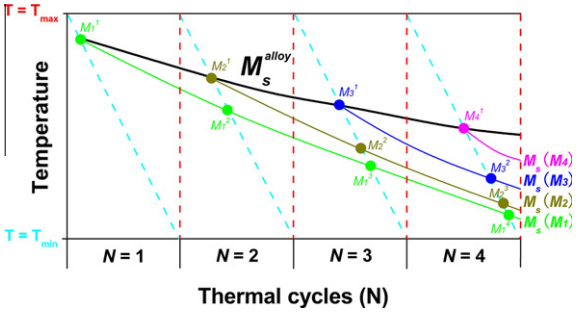

Fig. 8. Overall M_s^{alloy} of the schematic sample as well as the $M_s(M1)$, $M_s(M2)$, $M_s(M3)$, and $M_s(M4)$ in dependence of thermal cycles, where the cyan and red dashed lines indicate the temperature change (for clarity the heating part of each cycle is subtracted and shown as straight red lines).

Simon et al. [12] with one exception: we did not see fine dislocation loops emanating from ingrown dislocation lines. Instead we observed the formation of dislocations in dislocation-free regions. The schematic scenario in Fig. 6 suggests that dislocation loops nucleate at the tip of a propagating martensite needle. They are left behind when the martensite needle retreats on heating, Fig. 6c.

4.2. Formation of dislocation clusters

The TEM micrographs of dislocation substructures compiled in Fig. 4 suggest that more and more leaf-like dislocation clusters form as a result of thermal cycling. The TEM micrograph in Fig. 4b shows that dislocation leaves spread out from a central region marked with a white circle. It seems reasonable to assume that this region provides

good nucleation conditions for martensite needles. In the following we use the schematic illustration presented in Fig. 7 to rationalize the dislocation substructure shown in the TEM micrograph of Fig. 4b. The four columns of Fig. 7 represent four subsequent cooling and heating cycles. Fig. 7a shows elementary processes which occur during cooling. Fig. 7b schematically illustrates the microstructures after re-heating. We discuss the first cooling cycle in the left column of Fig. 7a. Picture 1-1 shows a defect-free austenitic grain interior where the circle represents a region which is favorable for nucleation of martensite needle. In picture 1-2, the temperature has decreased and the first martensite needle (represented by an arrow in picture 1-2) $M1^1$ has formed for the first time ($M1^1$: lower index 1 for the type of needle, upper index 1 for the first time of appearance). The formation of the martensite needle $M1^1$ is promoted by a unique combination of local chemical, crystallographic, microstructural, thermodynamic and micromechanic conditions. As can be seen in Fig. 8, the formation of $M1^1$ occurs at the martensite start temperature $M_s(M1^1)$. The thin lines which intersect the arrow of $M1^1$ schematically illustrate the dislocation cluster which forms, according to the scenario outlined in Fig. 6. After re-heating, the martensite needle $M1^1$ retreats and leaves the dislocation cluster behind, as is schematically illustrated in the first picture of Fig. 7b, referred to as 1-3, because it represents the third microstructure in the first cooling–heating cycle. The microstructure after the first cooling–heating cycle is the starting microstructure of the second cooling–heating cycle. In our schematic illustration, the microstructures 1-3 (end of the first cooling–heating cycle) and 2-1 (beginning of the second cooling–heating cycle) are identical. This is why the first image in Fig. 7b carries both reference numbers, 1-3 and 2-1.

So far we have assumed that the dislocations which appear in picture 1-2 accommodate the growth of the martensite needle $M1^1$. Our microstructural observation presented in Fig. 4b leaves no other possibility than to qualitatively suggest the following sequence of events. The dislocations which are left behind after the martensite needle $M1^1$ has retreated (picture 1-3/2-1), do not promote the formation and growth of a new martensite needle of type $M1$ in the next cycle. In the beginning of the second cooling cycle at a temperature lower than $M_s(M1^1)$, another needle $M2^1$ nucleates and grows as in picture 2-2. As is illustrated in Fig. 8, the martensitic transformation in our model system now starts at $M_s(M2^1)$. But only a little later, a needle of type $M1$ reappears, picture 2-3. It is now referred to as $M1^2$ (first type of needle which forms for the second time).

It is important that needles of type $M1$ reappear, because otherwise we could not explain the increase of the dislocation density in the leaves as documented in Fig. 5b. The unique conditions which made $M1^2$ appear in the first cycle have changed. And this must be due to the dislocations which have formed. These have now changed their role. Instead of making it easier for the $M1$ -type needle to reappear, as one may expect, they now make it more difficult. This is why martensite needle $M2^1$ forms in the beginning of the second cooling cycle before a needle of type $M1$ reappears. After this detailed description of the elementary transformation and local deformation processes in the first and second cooling cycles, it is easy to understand the order events which govern all subsequent heating–cooling cycles. The martensite start temperatures of martensite needles decrease due to the presence of the dislocations which have assisted their growth. Other needles benefit and grow before higher driving forces associated with more undercooling let the previous type of needles reappear. The further increase of dislocations around needles in subsequent cooling cycles results in decreasing martensite start temperature of needles (e.g. $M_s(M1^1) > M_s(M1^2) > M_s(M1^3) > M_s(M1^4)$, illustrated as curve $M_s(M1)$ in Fig. 8). And in each cooling cycle, another type of martensite needle governs the martensite start temperature of the whole system M_s^{alloy}, as shown in Fig. 8 (cycle 1: $M_s^{alloy} = M_s(M1^1)$, cycle 2: $M_s^{alloy} = M_s(M2^1) > M_s(M1^2)$, cycle 3: $M_s^{alloy} = M_s(M3^1) > M_s(M2^2) > M_s(M1^3)$ and so on).

Further work is required to provide an atomistic and micromechanical explanation for the described behavior. But the scenario outlined in Figs. 7 and 8 helps to rationalize both the DSC results (Fig. 1) and the TEM results (Fig. 4).

5. Conclusions

In the present study we investigate the evolution of dislocation substructures during thermal cycling of a coarse-grained Ti–50.6Ni alloy which was solutionized at 1273 K for 1 h. We document the decrease of the martensite start temperature, M_s^{alloy} during thermal cycling. In parallel we perform diffraction contrast transmission electron microscopy to assess the effect of martensitic transformation cycles on evolving dislocation substructures in the austenite (B2 phase). From the results obtained in the present study, the following conclusion can be drawn:

1. The macroscopic martensite start temperature M_s^{alloy} of a coarse-grained Ti–50.6Ni shape memory alloy decreases during thermal cycling.
2. This decrease of M_s^{alloy} is related to the formation of a unique dislocation substructure with leaf-like features, which has not been observed before.
3. A dislocation leaf forms around a martensite needle, which nucleates and further grows at its microscopic martensite start temperature M_s^{needle}. The macroscopic martensite start temperature of the system corresponds to the microscopic martensite start temperature of the needle which forms first.
4. Dislocations which form around a martensite needle to accommodate its growth during the cooling period of one cooling–heating cycle appear to impede the nucleation of the same type of needle in the cooling period

of the subsequent heating–cooling cycle. They do not fully suppress its reappearance, but they delay its formation and growth and thus other needles can nucleate and grow before. This explains, in a coarse-grained Ti–Ni alloy which undergoes functional fatigue during thermal cycling, the formation of the leaf-like dislocation substructure observed in the present study.

Acknowledgements

The present work was supported by A8 of SFB459 (Shape Memory Technology) funded by the Deutsche Forschungsgemeinschaft (DFG). The authors also acknowledge funding by the Alexander von Humboldt Foundation, the National Science Foundation of China (51171140), National Basic Research Program of China (2010CB613003 and 2012CB619401), 111 project of China (B06025), as well as the support from the Grant-in-Aid for Scientific Research b of JSPS. The authors thank J. Frenzel, Ph. Nörtershäuser and A. Aghajani for helpful discussions and technical support.

References

[1] Chang LC, Read TA. Trans AIME 1951;191:47.
[2] Wayman C. Introduction to the crystallography of martensitic transformations. New York: Macmillan; 1964.
[3] Honma T. Shape memory alloys. New York: Gordon & Breach Science; 1987.
[4] Otsuka K, Ren X. Prog Mater Sci 2005;50:511.
[5] Eggeler G, Hornbogen E, Yawny A, Heckmann A, Wagner M. Mater Sci Eng A 2004;378:24.
[6] Gall K, Maier H. Acta Mater 2002;50:4643.
[7] Miyazaki S, Imai T, Igo Y, Otsuka K. Metall Trans A 1986;17:115.
[8] Miyazaki S, Igo Y, Otsuka K. Acta Metall 1986;34:2045.
[9] McCormick PG, Liu YN. Acta Metall Mater 1994;42:2407.
[10] Nishida M, Yamauchi K, Itai I, Ohgi H, Chiba A. Acta Metall Mater 1995;43:1229.
[11] Ding XD, Suzuki T, Ren XB, Sun J, Otsuka K. Phys Rev B 2006:74.
[12] Simon T, Kroger A, Somsen C, Dhouy A, Eggeler G. Acta Mater 2010;58:1850.
[13] Frank FC. Acta Metall 1953;1:15.
[14] Pond RC, Celotto S, Hirth JP. Acta Mater 2003;51:5385.
[15] Grossmann C, Frenzel J, Sampath V, Depka T, Eggeler G. Metall Mater Trans A 2009;40A:2530.
[16] Olbricht J, Yawny A, Condo AM, Lovey FC, Eggeler G. Mater Sci Eng A 2008;481:142.
[17] Yawny A, Sade M, Eggeler G. Z Metall 2005;96:608.
[18] Chumlyakov YI, Efimenko SP, Kireeva IV, Panchenko EY, Sehitogly H, Gall K, et al. Dokl Phys 2001;46:849.
[19] Hamilton RF, Sehitoglu H, Chumlyakov Y, Maier HJ. Acta Mater 2004;52:3383.
[20] Ibarra A, San Juan J, Bocanegra EH, No ML. Acta Mater 2007;55:4789.
[21] Norfleet DM, Sarosi PM, Manchiraju S, Wagner MFX, Uchic MD, Anderson PM, et al. Acta Mater 2009;57:3549.
[22] Zhang J, Fan GL, Zhou YM, Ding XD, Otsuka K, Nakamura K, et al. Acta Mater 2007;55:2897.